Available online at www.sciencedirect.com
ScienceDirect
Journal of Sound and Vibration 320 (2009) 516–526
JOURNAL OF SOUND AND VIBRATION
www.elsevier.com/locate/jsvi

Characteristics of distributed parameter isolators

B. Yan, M.J. Brennan*, S.J. Elliott, N.S. Ferguson

Institute of Sound and Vibration Research, University of Southampton, Southampton SO17 1BJ, UK

Received 9 February 2008; received in revised form 28 July 2008; accepted 4 August 2008
Handling Editor: C.L. Morfey
Available online 1 October 2008

Abstract

The widely used traditional massless isolator model is only valid at relatively low frequencies. In this paper two classes of distributed parameter isolator, non-dispersive and dispersive, which are valid over a wide range of frequencies, are studied and compared. The important characteristics of such distributed parameter isolators in isolating a mass are given, as are the parameters which control the isolator performance at various frequencies. The theoretical findings for one distributed parameter isolator are validated experimentally using a helical spring, as an example of a non-dispersive isolator.

1. Introduction

In the treatment of vibration isolation, isolators are often considered as simple lumped parameter elements, which are assumed to be massless for the purpose of modelling [1–3]. The conventional massless isolator model is useful in that it provides basic guidelines for isolator design. However, this simplification is only valid at relatively low frequencies, for which the wavelength in the isolator is long compared to its dimension [4,5]. At higher frequencies the distributed mass, stiffness and damping in the isolator introduce dynamics, which are associated with the resonance behaviour of the isolator. These resonances are referred to as internal resonances or wave effects in the isolator [5–7]. This phenomenon is also known as spring surge in the area of spring design [8]. The predictions from the massless isolator model are, therefore, no longer accurate. Given the trend in many industries towards more complex equipment and machines, which are lighter and more compact, operating at higher speeds with higher power rating, higher frequency vibrations have become more important. As a consequence, it is necessary to provide vibration isolation systems that will remain effective at high frequencies. A model with distributed mass, stiffness and damping is thus needed.

The presence and importance of internal resonances has been known and investigated since the 1950s. Sykes [9] observed that the internal resonances occur in certain frequency ranges, when the wavelength of the exciting vibration in the isolator is comparable with the isolator's length. Ungar and Dietrich [6] noted that the wave effects are more important in a heavier and larger isolator than those in a lighter and smaller isolator of equal static stiffness. It was found that the internal resonances in an isolator are determined by various factors,

*Corresponding author.
E-mail address: mjb@isvr.soton.ac.uk (M.J. Brennan).

0022-460X/$ - see front matter © 2008 Elsevier Ltd. All rights reserved.
doi:10.1016/j.jsv.2008.08.011

e.g. the shape, material properties, dimensions, and boundary conditions of the isolators [5], as well as the type of deformation (e.g. compression, shear, flexure) [10]. The wave effects in the isolator can significantly degrade the isolator performance at high frequencies, especially for lightly damped metallic isolators, e.g. metal springs, since the smaller the loss factor in the isolator the more significant are the resonances caused by the wave effects [5,11]. Lee and Thompson [12] showed that the internal resonances lead to significant dynamic stiffening for helical springs above a certain frequency. This occurs at frequencies as low as about 40 Hz for an automotive suspension spring. Tomlinson [13] pointed out that it is especially necessary to consider the wave effects in metal springs for high frequency isolation design. It was shown analytically and experimentally that, in some situations, the lowest internal resonance in metal springs appears below 200 Hz and has almost the same amplitude as the fundamental system resonance.

Various distributed parameter models have been used to investigate the internal resonance problem. The idealised "long-rod" model for helical springs and cylindrical rubber isolators, which have simple geometries and deformation behaviour, has been widely used to investigate the wave effects in an isolator [5–7]. In this "long-rod" theory, the isolator is modelled as a continuous elastic finite rod with internal damping, which has mass characterized by the material density. Other distributed parameter models have also been studied, for example in Refs. [10,14]. Ungar [10] used a continuous uniform beam model to investigate the internal resonances in leaf springs operating in flexure.

Previous research on the internal resonance problem is, however, not particularly comprehensive, because it does not clarify all the important characteristics of isolators, such as the parameters which control the isolator performance at various important frequencies. The aim of this article is to fill this gap. Different distributed parameter models for the isolator are presented, and their characteristics in isolating a mass from base motion are investigated. The way in which the system parameters affect the response of the system at various frequencies are determined and two different classes of isolator are compared. Experimental work on a mass supported on a helical spring is presented to support the theoretical results.

2. Theoretical analysis

The types of distributed parameter isolators considered in this paper are shown in Fig. 1. Each isolator is considered as a one-dimensional system, subjected to base motion (longitudinal, torsional, or lateral vibration), and connects to an equipment structure at a single point.

These isolators can be categorized into two types for the purpose of dynamic analysis. One type can be modelled using a second-order partial differential equation, and is referred to here as a *non-dispersive isolator*, since the wave speed of interest is independent of frequency. The other type can be modelled using a fourth-order partial differential equation, and is referred to here as a *dispersive isolator*, since the wave speed of interest is dependent on frequency. The isolator in Fig. 1(a) is modelled as an elastic rod subject to longitudinal vibration, the isolator in Fig. 1(c) is modelled as an elastic shaft subject to torsional vibration, and the isolator in Fig. 1(e) is modelled as either a shear beam, or an Euler Bernoulli beam, depending on the dimensions and material properties of the beam. The rod, the shaft and the shear beam are examples of non-dispersive isolators, while the Euler Bernoulli beam is an example of a dispersive isolator.

A general frequency domain description of the isolators shown in Fig. 1 is given by

$$Q_e = Z_e \dot{u}_e \tag{1a}$$

and

$$\begin{bmatrix} Q_1 \\ Q_2 \end{bmatrix} = \mathbf{Z}_I \begin{bmatrix} \dot{u}_b \\ \dot{u}_e \end{bmatrix} \tag{1b}$$

where $\mathbf{Z}_I$ is the impedance matrix of the isolator, whose elements are given by

$$\mathbf{Z}_I = \begin{bmatrix} Z_{11} & Z_{12} \\ Z_{21} & Z_{22} \end{bmatrix}$$

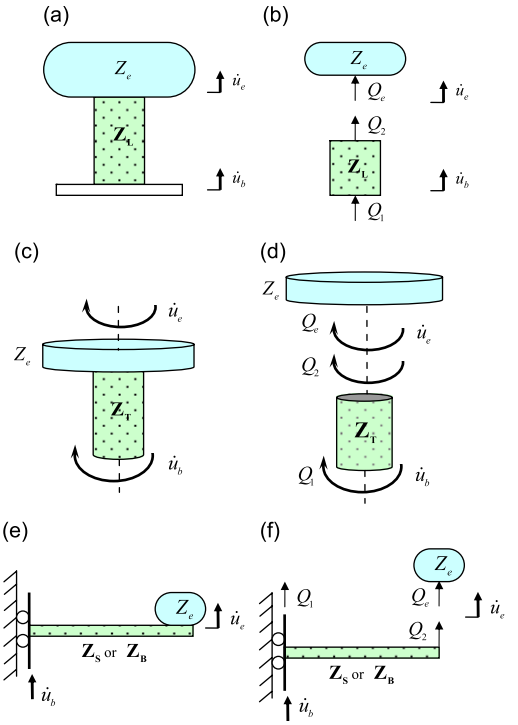

Fig. 1. Schematic diagrams of vibration isolation systems containing a distributed parameter isolator under (a) longitudinal, (c) torsional or (e) lateral vibration. (b), (d) and (f) are, respectively, free body diagrams. Q_e, Q_1 and Q_2 are internal forces in (b) and (f), or moments in (d); $\dot{u}_e$ and $\dot{u}_b$ are velocity in (b) and (f), or angular velocity (d) of the equipment and the base, respectively; Z_e is the input impedance of the equipment; $\mathbf{Z}_L$ and $\mathbf{Z}_T$ are the impedance matrices for the rod under longitudinal and torsional vibration, respectively; and $\mathbf{Z}_s$ and $\mathbf{Z}_B$ are the impedance matrices for the shear beam and Euler–Bernoulli beam, respectively.

and the internal forces or moments are given by Q_e, Q_1 and Q_2 as shown in Figs. 1(b),(d),(f); note that $Q_e = -Q_2$. The velocity or angular velocity of the equipment and the base are given by $\dot{u}_e$ and $\dot{u}_b$, respectively, and Z_e is the impedance of the equipment at the point where it is connected to the isolator. Referring to Fig. 1, for the rod, $\mathbf{Z}_L = \mathbf{Z}_I$, for the shaft $\mathbf{Z}_T = \mathbf{Z}_I$, for the shear beam $\mathbf{Z}_s = \mathbf{Z}_I$ and for the Euler–Bernoulli beam $\mathbf{Z}_B = \mathbf{Z}_I$. The transmissibility, which is defined as the ratio of the velocities (angular velocities) above and below the isolator, for all the systems shown in Fig. 1 has the same form, and can be determined using Eqs. (1a,b), to give

$$T = \frac{\dot{u}_e}{\dot{u}_b} = \frac{-Z_{21}}{Z_e + Z_{22}} \tag{2}$$

The transmissibilities of the isolators for the non-dispersive and dispersive isolators depicted in Fig. 1 are contrasted and compared in the following subsections.

2.1. Non-dispersive isolator

For an isolator that is long compared to its cross-sectional dimensions [15,16], subject to longitudinal vibration shown in Fig. 1(a), the impedance matrix is given by [17,18]

$$\mathbf{Z}_L = \frac{S\sqrt{E^*\rho}}{\mathrm{j}\sin(k_l^* L)} \begin{bmatrix} \cos(k_l^* L) & -1 \\ -1 & \cos(k_l^* L) \end{bmatrix} \tag{3}$$

where L, S and ρ are the length, cross-sectional area and density of the isolator, respectively. The complex Young's modulus E^* is given by $E^* = E(1+\mathrm{j}\eta_l)$, where η_l is the loss factor and $\mathrm{j} = \sqrt{(-1)}$. The complex

longitudinal wavenumber is given by $k_l^* \approx k_l(1 - j\eta_l/2)$, where $k_l = \sqrt{\rho/E}\omega$ is the longitudinal wavenumber of the undamped isolator, and ω is the angular frequency.

For the isolator subject to torsional vibration shown in Fig. 1(c), the impedance matrix is given by [17,18]

$$\mathbf{Z}_T = \frac{J_s\sqrt{G^*\rho}}{j\sin(k_s^*L)}\begin{bmatrix}\cos(k_s^*L) & -1\\ -1 & \cos(k_s^*L)\end{bmatrix} \tag{4}$$

where J_s is the polar second moment of area of the isolator; $G^* = G(1+j\eta_s)$ is the complex shear modulus, where η_s is the shear loss factor; $k_s^* \approx k_s(1-j\eta_s/2)$ is the complex shear wavenumber, where $k_s = \sqrt{\rho/G}\omega$ is the shear wavenumber in the undamped isolator.

Similarly, for the shear beam isolator subject to lateral vibration in Fig. 1(e), the impedance matrix is given by [19]

$$\mathbf{Z}_s = \frac{S\sqrt{G^*\rho}}{j\sin(k_s^*L)}\begin{bmatrix}\cos(k_s^*L) & -1\\ -1 & \cos(k_s^*L)\end{bmatrix} \tag{5}$$

Henceforth it is assumed that the equipment is mass-like so that in Figs. 1(a) and (e), $Z_e = j\omega m_e$, where m_e is the mass of the equipment, and $Z_e = j\omega J_e$, where J_e is the polar moment of inertia of the equipment in Fig. 1(c). Substituting the appropriate impedances from Eqs. (3)–(5) into Eq. (2), the transmissibility of a non-dispersive isolator can be written in non-dimensional form as

$$T = \frac{1}{\cos\left[\sqrt{\mu}(1 - j(\eta/2))\Omega\right] - (\Omega/\sqrt{\mu})(1 - j(\eta/2))\sin\left[\sqrt{\mu}(1 - j(\eta/2))\Omega\right]} \tag{6}$$

where $\Omega = \omega/\omega_e$ is the normalised frequency, i.e. the ratio of the excitation frequency ω to the system fundamental natural frequency ω_e, due to the interaction of the equipment mass and the static stiffness of the isolator. For the longitudinal isolator, $\omega_e = \sqrt{K_L/m_e}$ where $K_L = ES/L$ is the static longitudinal stiffness of the isolator; $\mu = \rho SL/m_e$ is the ratio of the mass of the isolator to the mass of the equipment. For the torsional isolator, $\omega_e = \sqrt{K_T/J_e}$ where $K_T = GJ_s/L$ is the static torsional stiffness of the isolator; $\mu = \rho J_s L/J_e$ is the ratio of the polar moment of inertia of the isolator to the polar moment of inertia of the equipment. For the shear beam isolator, $\omega_e = \sqrt{K_s/m_e}$ where $K_s = GS/L$ is the static shear stiffness of the isolator and $\mu = \rho SL/m_e$. It is also assumed that $\eta = \eta_l = \eta_s$.

The transmissibility of the vibration isolation systems with a non-dispersive isolator is plotted in Fig. 2 for the case when $\mu = 0.1$ and $\eta = 0.001$. For comparison, the transmissibility of a system containing a massless isolator is also plotted. It can be seen that the transmissibility for a non-dispersive isolator has a peak at a frequency close to that of the fundamental resonance for a massless isolator.

However, at high frequencies ($\Omega \gg 1$), the transmissibility for the system with a non-dispersive isolator is greater than that for the massless isolator because of the internal resonances in the isolator. Two other lines are plotted: one which passes through the peaks of the internal resonances, here called a "peak" line and one which passes through the troughs, called a "trough" line. The circle corresponds to the frequency at which the transmissibility for a non-dispersive isolator and that for a massless isolator start to deviate, i.e., the frequency above which wave effects in the isolator becomes detrimental to the performance of the isolator. Approximate expressions for these lines and this point are determined below, as they give physical insight into the parameters that govern the dynamic behaviour of the isolator.

To determine the "peak" line it is first noted that the peaks in the transmissibility occur approximately at a natural frequency of the isolator, i.e. when $\sin(\sqrt{\mu}\Omega) = 0$. Thus, the sin and cos terms in Eq. (6), can be expanded, and $\sin(\sqrt{\mu}\Omega)$ set to zero and $\cos(\sqrt{\mu}\Omega)$ set to 1. Also, it can be assumed that $\eta\sqrt{\mu}\Omega/2 \ll 1$, because $\eta \ll 1$ and $\mu \ll 1$, so that small angle approximations can be made so that $\cos(j\eta\sqrt{\mu}\Omega/2) \approx 1$ and $\sin(j\eta\sqrt{\mu}\Omega/2) \approx j\eta\sqrt{\mu}\Omega/2$. Eq. (6) can thus be approximated to

$$T_{\text{peak}} \approx \frac{1}{1 + (j/2)\eta\Omega^2} \tag{7}$$

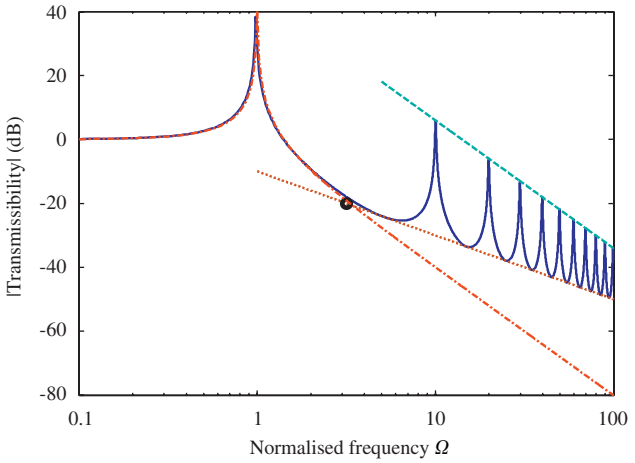

Fig. 2. Transmissibility of the vibration isolation systems with a non-dispersive isolator when $\mu = 0.1$ and $\eta = 0.01$ (solid line). The dashed line passes through the internal resonance peaks, $|T|_{\text{peak}}$. The dotted line passes through the troughs in the transmissibility, $|T|_{\text{trough}}$. The dashed-dotted line is for the massless isolator. The point circled is the intersection of the transmissibility for the system with a massless isolator and for the "trough" line, Ω_c. It denotes the point at which the transmissibility of the distributed parameter isolator starts to deviate from the massless isolator, and for which the transmissibility equals $|T|_c$.

which can be further approximated by noting that at high frequencies ($\Omega \gg 1$) the imaginary term in the denominator dominates, so that the "peak" line is given by

$$|T|_{\text{peak}} \approx \frac{2}{\eta}\frac{1}{\Omega^2} \tag{8}$$

It can be seen that the "peak" line is governed by the loss factor η and frequency ratio Ω. It decreases at a rate of 40 dB per decade. Thus, increasing the damping in the isolator or decreasing the system fundamental resonance frequency, e.g. by increasing the isolator length and hence reducing its stiffness, are effective ways of attenuating the internal resonance peaks.

To determine the "trough" line it is noted that a trough occurs approximately when $\sin(\sqrt{\mu}\Omega) = 1$ and when $\cos(\sqrt{\mu}\Omega) = 0$. Again, expanding the sin and cos terms in Eq. (6), applying these conditions, and using small angle approximations gives

$$|T|_{\text{trough}} \approx \sqrt{\mu}\frac{1}{\Omega} \tag{9}$$

which is a function of the ratio μ and frequency ratio Ω. The trough line decreases at a rate of 20 dB per decade, compared to that of 40 dB per decade for the massless isolator. Examination of Fig. 2 shows that at high frequencies, well above the fundamental resonance frequency, the transmissibility for the distributed parameter isolator generally decreases at a lower rate than that for the massless isolator due to the internal resonances.

Substituting for the appropriate μ and Ω into Eq. (9) gives

$$|T|_{\text{trough}} \approx \frac{S\sqrt{E\rho}}{\omega m_e} \quad \text{or} \quad \frac{J_s\sqrt{G\rho}}{\omega J_e} \quad \text{or} \quad \frac{S\sqrt{G\rho}}{\omega m_e} \tag{10a,b,c}$$

for the rod, the shaft and the shear beam, respectively. It is evident that the "trough" line is independent of the isolator length. Thus, to improve the performance of the isolation system, the isolator mass, polar moment of inertia or fundamental natural frequency can be adjusted by changing the isolator parameters except for the length.

To determine the frequency Ω_c, at which the transmissibility for a non-dispersive isolator and that for a massless isolator start to deviate, the line that passes though the troughs given by Eq. (9) is set to be equal to

the magnitude of the transmissibility for an undamped massless isolator at high frequencies ($\Omega \gg 1$), given by $|T|_{\text{massless}} \approx 1/\Omega^2$ to give

$$\Omega_c \approx \frac{1}{\sqrt{\mu}} \tag{11}$$

and the transmissibility at this frequency is given by

$$|T|_c \approx \mu \tag{12}$$

This shows that the ratio of the mass or the polar moment of inertia of the isolator to that of the equipment is crucial to the performance of the isolator. In general, the lighter the isolator, the better the high frequency performance, because the onset of the internal resonances is shifted to higher frequencies.

2.2. Dispersive isolator

The dispersive isolator (that is long compared to its cross-sectional dimensions) considered here is shown in Fig. 1(e). It is represented by an Euler–Bernoulli beam undergoing lateral vibration. For the sake of simplicity it is assumed that one end of the isolator slides under external excitation, and the equipment, represented by impedance Z_e, is connected through a pinned joint at the other end.

For a sliding-free Euler–Bernoulli beam, there is no rotation at the sliding end and there is no bending moment at the free end, so the impedance matrix is given by [20]

$$\mathbf{Z}_B = \begin{bmatrix} Z_{11} & Z_{12} \\ Z_{21} & Z_{22} \end{bmatrix} \tag{13}$$

where

$$Z_{11} = \frac{2E^*Ik_b^{*3}\cos(k_b^*L)\cosh(k_b^*L)}{\mathrm{j}\omega(\sin(k_b^*L)\cosh(k_b^*L) - \cos(k_b^*L)\sinh(k_b^*L))}$$

$$Z_{12} = Z_{21} = -\frac{E^*Ik_b^{*3}(\cos(k_b^*L) + \cosh(k_b^*L))}{\mathrm{j}\omega(\sin(k_b^*L)\cosh(k_b^*L) - \cos(k_b^*L)\sinh(k_b^*L))}$$

$$Z_{22} = \frac{E^*Ik_b^{*3}(1 + \cos(k_b^*L)\cosh(k_b^*L))}{\mathrm{j}\omega(\sin(k_b^*L)\cosh(k_b^*L) - \cos(k_b^*L)\sinh(k_b^*L))}$$

in which I is the second moment of area about the neutral axis of the isolator, $k_b^* \approx k_b(1-\mathrm{j}\eta_i/4)$, is the bending wavenumber in the isolator, where $k_b = \sqrt[4]{\rho S/EI}\,\sqrt{\omega}$ is the wavenumber of an undamped isolator.

If the equipment is assumed to have a mass-like impedance, i.e. $Z_e = \mathrm{j}\omega m_e$, and the appropriate impedances in Eq. (13) are substituted into Eq. (2), the transmissibility can be written in a non-dimensional form as

$$T = \frac{1}{\dfrac{1+\cos\gamma^*\cosh\gamma^*}{\cos\gamma^*+\cosh\gamma^*} - \sqrt[4]{\dfrac{3\Omega^2}{\mu^3}}\left(1-\dfrac{\mathrm{j}\eta}{4}\right)\dfrac{\sin\gamma^*\cosh\gamma^* - \cos\gamma^*\sinh\gamma^*}{\cos\gamma^*+\cosh\gamma^*}} \tag{14}$$

where $\gamma^* = \gamma(1-\mathrm{j}\eta_i/4)$, in which $\gamma = \sqrt[4]{3\mu\Omega^2}$ and $\Omega = \omega/\omega_e$ is the ratio of the excitation frequency ω to the system fundamental natural frequency ω_e; $\omega_e = \sqrt{K_B/m_e}$ where $K_B = 3EI/L^3$ is the static bending stiffness of the isolator; $\mu = \rho SL/m_e$ is the ratio of the mass of the isolator to the mass of the equipment.

The transmissibility of the vibration isolation system with a dispersive isolator is plotted in Fig. 3 for $\mu = 0.1$ and $\eta = 0.01$. For comparison, the transmissibility of a system containing a massless isolator is also plotted. Similar characteristic lines to those in Fig. 2 are also depicted.

To determine the "peak" line, it is first noted that at high frequencies when $\gamma \gg 1$, then $\sinh\gamma^* \approx \cosh\gamma^* \gg 1$. Provided that damping is small such that $\eta \ll 1$, Eq. (14) reduces to

$$T \approx \frac{1}{\cos\gamma^* - \sqrt[4]{(3\Omega^2/\mu^3)}(\sin\gamma^* - \cos\gamma^*)} \tag{15}$$

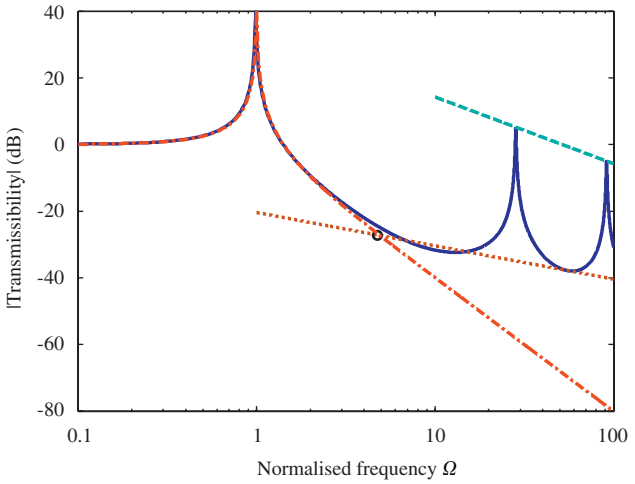

Fig. 3. Transmissibility of the passive vibration isolation system with a dispersive isolator when $\mu = 0.1$ and $\eta = 0.01$ (solid line). The dashed line passes through the internal resonance peaks. The dotted line passes through the troughs in the transmissibility. The dashed-dotted line is for the massless isolator. The point circled is the intersection of the transmissibility for the system with a massless isolator and the "trough" line.

The high-order natural frequencies of the sliding-free beam, which are the approximate frequencies at which the peaks in the transmissibility due to internal resonances in the isolator, occur when $\sin\gamma \approx \cos\gamma = 1/\sqrt{2}$. Using this fact, and assuming small angle approximations results in

$$|T|_{\text{peak}} \approx \sqrt{\frac{2\mu}{3}}\frac{2}{\eta}\frac{1}{\Omega} \tag{16}$$

It can be seen that this differs from the "peak" line for the non-dispersive isolator given in Eq. (8) in that it is a function of the mass ratio, and that it is a also proportional to $1/\Omega$ rather than $1/\Omega^2$, which means that the peaks in the internal resonances decrease at a rate of 20 dB per decade, rather than 40 dB per decade for the non-dispersive isolator. Substituting the appropriate μ and Ω into Eq. (16) gives

$$|T|_{\text{peak}} \approx \frac{\sqrt{2EI\rho S}}{m_e L}\frac{2}{\eta}\frac{1}{\omega} \tag{17}$$

which shows that to suppress the peaks, the isolator mass can be adjusted by reducing its density or cross-section area. Moreover, the peaks can also be reduced by increasing the length of the isolator, which is the same as for the non-dispersive isolator discussed above.

The line through the troughs in the transmissibility can be determined by noting that Eq. (15) has a minimum when ($\sin\gamma^*$–$\cos\gamma^*$) is maximum, which is when $|\sin\gamma^* - \cos\gamma^*|_{\max} = \sqrt{2}$. Eq. (15), then becomes

$$|T|_{\text{trough}} \approx \sqrt[4]{\frac{\mu^3}{12}}\frac{1}{\sqrt{\Omega}} \tag{18}$$

which is a function of the mass ratio μ and frequency ratio Ω as in the case of the non-dispersive isolator. However, the mass ratio has a greater effect in this case and the "trough" line decreases at a rate of 10 dB per decade, compared to the rate of 40 dB per decade for the massless isolator and 20 dB per decade for the non-dispersive isolator. Substituting the appropriate μ and Ω into Eq. (18) gives

$$|T|_{\text{trough}} \approx \sqrt[4]{\frac{EI(\rho S)^3}{4}}\frac{1}{m_e}\frac{1}{\sqrt{\omega}} \tag{19}$$

It can be seen that the "trough" line is again independent of the isolator length. Therefore, to improve the performance of the isolator its mass or natural frequency can be adjusted by changing the isolator parameters, except for the length.

Table 1
Characteristics of distributed parameter isolators undergoing base motion, where Ω is the normalised frequency, η is the loss factor in the isolator and μ is the ratio of the mass or polar moment of inertia of the isolator to the mass or polar moment of inertia of the equipment

Isolator type	$\lvert T\rvert_{\text{peak}}$	$\lvert T\rvert_{\text{trough}}$	$(\Omega_c, \lvert T\rvert_c)$
Non-dispersive isolator	$\frac{2}{\eta}\frac{1}{\Omega^2}$	$\sqrt{\mu}\frac{1}{\Omega}$	$\left(\frac{1}{\sqrt{\mu}}, \mu\right)$
Dispersive isolator	$\sqrt{\frac{2\mu}{3}}\frac{2}{\eta}\frac{1}{\Omega}$	$\sqrt[4]{\frac{\mu^3}{12}\frac{1}{\sqrt{\Omega}}}$	$\left(\sqrt[6]{12}\frac{1}{\sqrt{\mu}}, \frac{1}{\sqrt[3]{12}}\mu\right)$

To determine the frequency Ω_c, at which the transmissibility for a dispersive isolator and that for a massless isolator start to deviate, the same procedure as before is carried out. Eq. (19) is set to be equal to $|T|_{\text{massless}} \approx 1/\Omega^2$ to give

$$\Omega_c \approx \sqrt[6]{12}\frac{1}{\sqrt{\mu}} \tag{20}$$

and the transmissibility at this frequency is given by

$$|T|_c \approx \frac{1}{\sqrt[3]{12}}\mu \tag{21}$$

which is only a function of the mass ratio μ. Similar to the non-dispersive isolator, it shows that the lighter the isolator, the better the isolator performance.

2.3. Summary

The main results from the analysis of the passive vibration isolation systems containing either a non-dispersive isolator or a dispersive isolator are summarised in Table 1. These are the line though the peaks in the transmissibility, the line though the troughs and the point at which the distributed parameter isolator starts to deviate from that of a massless isolator. It is clear that three factors are crucial to the performance of the isolation system, namely the ratio μ, the isolator loss factor η and the frequency ratio Ω. The differences between the non-dispersive isolators and the dispersive isolator are also clear. Compared to the non-dispersive isolator, the internal resonances for the dispersive isolator have a lower density with respect to frequency and occur at much higher non-dimensional frequencies. Generally, in practice, the internal resonances in the dispersive isolator can be attenuated to a greater extent compared to those in the non-dispersive isolator, since damping can be incorporated more easily into dispersive isolators, e.g. flexural springs [10]. Thus, in practice the undesirable effects of internal resonances on the isolation performance for the non-dispersive isolator are more significant than that for the dispersive isolator.

3. Experimental work

To validate some of the modelling work an experiment was conducted on a mass supported on a helical spring as shown in Fig. 4. A helical spring can be modelled crudely as an equivalent finite elastic rod subject to longitudinal vibration [5,7].

The system was excited at the base using an electromagnetic shaker (LDS V201) driven by a white noise generator as shown in Fig. 4. The characteristic properties of the equipment and the helical spring are listed in Table 2. Three accelerometers (PCB type 352C22) were attached symmetrically to the isolated mass to measure its response. The outputs of these three accelerometers were averaged to eliminate the effect of any rotation. One accelerometer was attached at the base of the helical spring to sense acceleration of the base, so that the transmissibility of the system could be measured. A dynamic signal analyser (Data Physics-Signalcalc Mobilyzer II) was used to both drive the system through a power amplifier (Ariston AX-910) and acquire the acceleration data above and below the isolator.

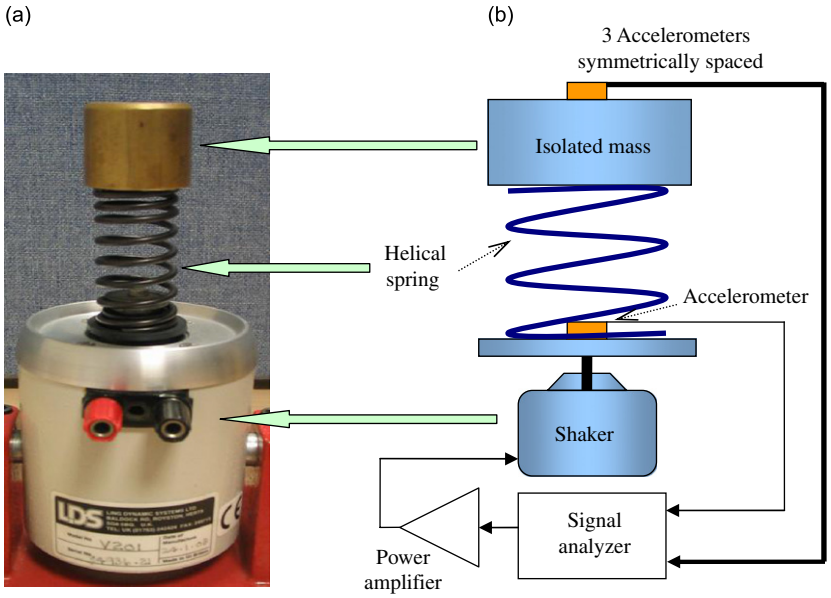

Fig. 4. (a) Photograph and (b) schematic diagram of the experimental rig of a mass supported by a helical spring undergoing base motion.

Table 2
Characteristic properties of the experimental rig on a helical spring

Mass of the equipment	193.1 g (measured)
Shear modulus of the spring	$7.93 \times 10^{10}\,\mathrm{N/m^2}$ (supplier data)
Density of the spring	$7900\,\mathrm{kg/m^3}$ (supplier data)
Wire diameter of the spring	2.6 mm (supplier data)
Mean diameter of the coil of the spring	24 mm (supplier data)
Number of complete coils of the spring	7.6 (supplier data)
Number of active coils of the spring	5.6 (supplier data)

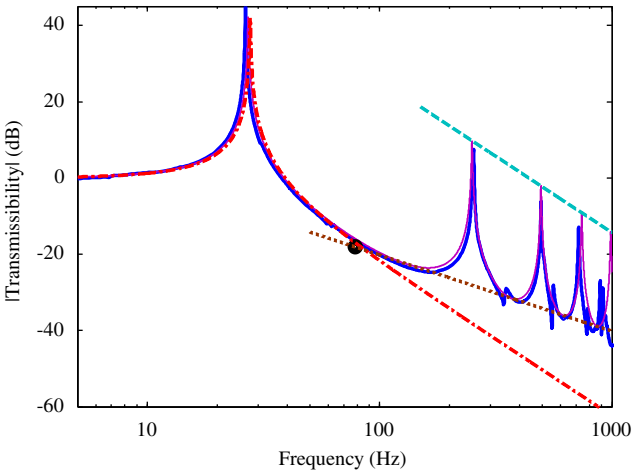

Fig. 5. Measured (solid bold) and predicted (solid faint) transmissibility of the experimental rig when $\mu = 0.125$ and $\eta = 0.008$. The dashed line passes through the internal resonance peaks. The dotted line passes through the troughs in the transmissibility. The dashed-dotted line is for the massless isolator. The point circled is the intersection of the transmissibility for the system with a massless isolator and for the "trough" line.

The measured transmissibility is shown in Fig. 5. Also shown in Fig. 5 are the predictions using the theoretical model described in the previous section. The predicted results can be obtained by substituting for the static stiffness of the helical spring and the ratio of the mass of the spring to the mass of the equipment into the corresponding equations. The static stiffness of a helical spring is given by [21]

$$K_s = \frac{Gd^4}{8nD^3} \tag{22}$$

where G is the shear modulus, d and D are wire diameter and mean diameter of the coil, respectively, and n is the number of active coils of the helical spring. The mass of the helical spring is given by

$$m_s = \frac{\pi^2 \rho N D d^2}{4} \tag{23}$$

where ρ and N are the density and the number of complete coils of the spring, respectively. Thus the ratio of the mass of the helical spring to the mass of the equipment is given by $\mu = \pi^2 \rho N D d^2 / 4 m_e$. Furthermore, the longitudinal internal resonance frequencies in a helical spring are given by

$$\omega_s = n\pi \sqrt{\frac{K_s}{m_s}} (\text{in rad/s}) \quad (n = 1, 2, 3 \ldots) \tag{24}$$

Using the parameters in Table 2, the static stiffness K_s was calculated to be 5851 N/m and the mass ratio μ used in the experiment was 0.125. A loss factor $\eta = 0.008$ for the isolator was used in the predictions.

Fig. 5 also shows the predicted transmissibility with the characteristic lines and point of intersection. The first three internal resonances in the helical spring can clearly be observed between 200 and 800 Hz, which are all well predicted. The experimental results agree reasonably well with the prediction, although there are some small measured peaks between the resonance peaks possibly due to rotational motion. The undesirable effects of internal resonances in the distributed parameter isolator on the isolation performance compared to a massless isolator are clearly shown in the experimental results, with the transmissibility being greater than unity at the first internal resonance, as well as at the fundamental mounted resonance frequency. In addition, this result demonstrates that an equivalent elastic finite rod is a reasonable representation for the distributed parameter model for a helical spring for longitudinal motion. The simple characteristic expressions given in Table 1 predict and describe the isolation performance of the experimental distributed parameter isolator fairly accurately.

4. Summary

In this paper, distributed parameter models for different isolator configurations have been studied. The isolators were categorized into two types, namely a non-dispersive isolator and a dispersive isolator. It has been shown that the isolation performance is significantly affected by the internal resonances in both types of isolator. Simple expressions which characterise the behaviour for distributed parameter isolators have been derived and presented in tabular form for ease of reference. Three non-dimensional parameters are crucial in the isolation of a mass on a distributed isolator; they are the mass (polar moment of inertia) ratio, the loss factor in the isolator and the non-dimensional frequency. Some experimental work has been conducted to support the theoretical predictions.

References

[1] S.S. Rao, *Mechanical Vibrations*, Addison-Wesley, Reading, MA, 1984.
[2] C.E. Crede, J.E. Ruzicka, Theory of vibration isolation, in: C.M. Harris, A.G. Piersol (Eds.), *Shock and Vibration Handbook*, McGraw-Hill, New York, 2002.
[3] C.R. Fuller, S.J. Elliott, P.A. Nelson, *Active Control of Vibration*, Academic Press, New York, 1996.
[4] M.J. Brennan, N.S. Ferguson, Vibration control, in: F.J. Fahy, J.G. Walker (Eds.), *Advanced Applications in Acoustics, Noise and Vibration*, E & FN SPON, London, 2004.
[5] M. Harrison, A.O. Sykes, M. Martin, Wave effects in isolation mounts, *Journal of the Acoustical Society of America* 24 (1952) 62–71.
[6] E.E. Ungar, C.W. Dietrich, High-frequency vibration isolation, *Journal of Sound and Vibration* 4 (1966) 224–241.

[7] J.C. Snowdon, Vibration isolation: use and characterization, *Journal of the Acoustical Society of America* 66 (1979) 1245–1274.
[8] J.E. Shigley, C.R. Mische, R. Budynas, *Mechanical Engineering Design*, seventh ed., McGraw-Hill, New York, 2003.
[9] A.O. Sykes, Isolation of vibration when machine and foundation are resilient and when wave effects occur in the mount, *Noise Control* 6 (1960) 115–130.
[10] E.E. Ungar, Wave effects in viscoelastic leaf and compression spring mounts, *Transactions of the American Society of Mechanical Engineers, Journal of Engineering for Industry* 85 (1963) 243–246.
[11] B. Yan, M.J. Brennan, S.J. Elliott, N.S. Ferguson, Velocity feedback control of vibration isolation systems containing a distributed parameter isolator, *Proceedings of the Ninth International Conference on Recent Advances in Structural Dynamics*, Southampton, UK, Paper 68, CD-ROM, 2006.
[12] J. Lee, D.J. Thomson, Dynamic stiffness formulation, free vibration and wave motion of helical springs, *Journal of Sound and Vibration* 239 (2001) 297–320.
[13] G.R. Tomlinson, Vibration isolation in the low and high frequency range, *Proceedings of Dynamic Vibration and Absorption Conference*, Southampton, UK, 1982, pp. 21–29.
[14] A. Sorensen, A discussion of the vibration characteristics of a simple mechanical connection, *Transactions of the American Society of Mechanical Engineers, Journal of Engineering for Industry* 82 (1960) 415–422.
[15] L. Kari, On the waveguide modelling of dynamic stiffness of cylindrical vibration isolators. Part I: The model, solution and experimental comparison, *Journal of Sound and Vibration* 244 (2) (2001) 211–233.
[16] L. Kari, On the waveguide modelling of dynamic stiffness of cylindrical vibration isolators. Part II: The dispersion relation solution, convergence analysis and comparison with simple models, *Journal of Sound and Vibration* 244 (2) (2001) 235–257.
[17] P. Gardonio, M.J. Brennan, Mobility and impedance methods in structural dynamics, in: F.J. Fahy, J.G. Walker (Eds.), *Advanced Applications in Acoustics, Noise and Vibration*, E & FN SPON, London, 2004.
[18] R.E.D. Bishop, D.C. Johnson, *The Mechanics of Vibration*, Cambridge University Press, Cambridge, 1960.
[19] B. Rafezy, W.P. Howson, Exact natural frequencies of a three-dimensional shear-torsion beam with doubly asymmetric cross-section using a two-dimensional approach, *Journal of Sound and Vibration* 295 (2006) 1044–1059.
[20] B. Yan, Active Vibration Isolation with a Distributed Parameter Isolator, PhD Thesis, University of Southampton, 2007.
[21] W.F. Stokey, Vibration of systems having distributed mass and elasticity, in: C.M. Harris, A.G. Piersol (Eds.), *Shock and Vibration Handbook*, McGraw-Hill, New York, 2002.